

Experimental and theoretical study of the structural environment of magnesium in minerals and silicate glasses using X-ray absorption near-edge structure

Nicolas Trcera · Delphine Cabaret ·
Stéphanie Rossano · François Farges ·
Anne-Marie Flank · Pierre Lagarde

Received: 25 July 2008 / Accepted: 30 September 2008 / Published online: 28 October 2008
© Springer-Verlag 2008

Abstract X-ray absorption spectroscopy at the Mg *K*-edge is used to obtain information on magnesium environment in minerals, silicate and aluminosilicate glasses. First-principles XANES calculations are performed for minerals using a plane-wave density functional formalism with core-hole effects treated in a supercell approach. The good agreement obtained between experimental and theoretical spectra provides useful information to interpret the spectral features. With the help of calculation, the position of the first peak of XANES spectra is related to both coordination and polyhedron distortion changes. In aluminosilicate glasses, magnesium is found to be mainly 5-fold coordinated to oxygen whatever the aluminum saturation index value. In silicate glasses, magnesium coordination increases from 4 in Cs-, Rb- and K-bearing glasses to 5 in Na- and Li-bearing glasses but remains equal as the polymerization degree of the glass varies. The variation of the C feature (position and intensity) is

strongly related to the alkali type providing information on the medium range order.

Keywords Magnesium · X-ray absorption spectroscopy · XANES · Ab initio calculation · Minerals · Glasses

Introduction

Magnesium is a major element of most natural compounds and can be as abundant as silica in undifferentiated primitive magmas. It has thus probably played an important role in the differentiation of the primitive Earth. At lower concentration, magnesium modifies glass properties as viscosity, glass transition temperature (Dingwell 1995) or the transmission window of light in car windows (Lefrère 2002). Concerning the durability properties, it has been found that the weathering rate of nuclear waste glasses is significantly increased when Mg is present (Curti 2003). However, in silicate glasses containing sodium and alkaline earth, Ca^{2+} and Mg^{2+} do not decrease the glass durability, unlike other alkaline earth (Koenderink et al. 2000). Despite this similarity, experimental studies have evidenced distinct behaviors for the two cations. For instance, the substitution of Na^+ by Ca^{2+} in silicate glasses leads to a linear variation of the glass transition temperature, unlike the substitution by Mg^{2+} (Branda et al. 1983). In bioactive glasses, magnesium seems to play a fundamental role in growth and dissolution of apatite crystals (Jallot 2003). The complete understanding of the effect of magnesium on these properties necessitates a precise knowledge of the structural environment of magnesium in glasses and of the competition between cations.

Despite its geochemical and technological importance, the environment of magnesium has been slightly studied

N. Trcera · S. Rossano (✉)
Laboratoire Géomatériaux et Géologie de l'Ingénieur (G2I),
Université Paris-Est, EA 4119, 5 bd Descartes,
77454 Marne la Vallée Cedex 2, France
e-mail: rossano@univ-mlv.fr

D. Cabaret
IMPMC, UMR7590, Universités Paris 6 et 7,
CNRS, IPGP, 140 rue de Lourmel, 75015 Paris, France

F. Farges
Laboratoire de Minéralogie (USM 201),
Muséum National d'Histoire Naturelle, CNRS UMR 7160,
61 rue Buffon, 75005 Paris, France

A.-M. Flank · P. Lagarde
CNRS UR1 Soleil, BP 48, 91192 Gif sur Yvette, France

due to both the refractory character of the concerned systems and technical difficulties to obtain reliable signals. The structural environment of magnesium in minerals, silicate melts and glasses has been investigated by different spectroscopies, such as ^{25}Mg magic angle spinning nuclear magnetic resonance (MAS NMR) which predicts four-, five- and six-fold coordinated Mg in various glass compositions (Fiske and Stebbins 1994; George and Stebbins 1998; Kroeker and Stebbins 2000), neutron and X-ray diffraction that revealed five-fold coordinated Mg in Mg_2SiO_4 and $\text{Mg}_2\text{Si}_2\text{O}_6$ glasses (Wilding et al. 2004) and in the $\text{MgO}-\text{Al}_2\text{O}_3-\text{SiO}_2$ glass system (Guignard and Cormier 2008). Besides these experimental methods, molecular dynamics (MD) simulations lead to four-fold and five-fold Mg in a MgSiO_3 glass (Kubicki and Lasaga 1991), and more recently Reverse Monte-Carlo calculations (Guignard and Cormier 2008) and molecular dynamics simulations (Guillot and Sator 2007) have confirmed the presence of five-fold Mg in aluminosilicate glasses.

XANES spectroscopy is a promising technique in order to investigate the structural environment of magnesium in silicate glasses, thanks to its chemical selectivity. As shown by multiple scattering calculations performed at the Mg *K*-edge in minerals (Cabaret et al. 1998; Wu et al. 2004), it is sensitive to local and medium range order up to about 7 Å around Mg. Moreover, this spectroscopy does not require specific sample preparation contrary to MAS NMR which requires ^{25}Mg isotope enrichment. However, Mg *K*-edge absorption studies are not so frequent in the literature, notably because of the technical difficulty of obtaining synchrotron beams with sufficient brilliance and monochromaticity in the 1,300–1,400 eV energy range where the Mg *K*-edge occurs (the 1s binding energy of Mg in its natural form is 1,303 eV (Thompson et al. 2001)). Mg *K*-edge XANES spectroscopy has been used in oxide and silicate minerals in order to define the fingerprint of the Mg coordination number on the spectra (Brown et al. 1995; Ildefonse et al. 1995; Andraut et al. 1998; Li et al. 1999). Mg *K*-edge XANES have been also carried out in pyroxenes (Cabaret et al. 1998), in olivine minerals (Wu et al. 2004), and in fibrous clay minerals (Sánchez del Río et al. 2005), in order to characterize the local atomic arrangement of Mg. Very recently, a Mg *K*-edge XANES and EXAFS (extended X-ray absorption fine structure) study in pyrope-grossular garnets has been reported (Quartieri et al. 2008). To our knowledge, in silicate glasses, the Mg *K*-edge studies only concern the system $\text{CaMgSi}_2\text{O}_6-\text{NaAlSi}_3\text{O}_8$ (Ildefonse et al. 1995; Li et al. 1999). Besides the experimental difficulties, the interpretation of XANES spectra is not straightforward and often requires first-principles theoretical tools. Mg *K*-edge calculations have been essentially performed on crystalline compounds within the

framework of multiple scattering theory, that uses the $Z + 1$ approximation to model the core-hole-electron interaction and a *muffin-tin* formulation of the electronic potential (Cabaret et al. 1998; Andraut et al. 1998; Wu et al. 2004). Recently we have shown that the agreement with experiment is systematically improved by using a full potential calculated self-consistently for a system including explicitly the absorbing atom 1s core-hole (Trcera et al. 2007). As an example, the Mg *K*-edge in MgO, that remains particularly difficult to calculate within multiple scattering theory, is very well reproduced by using full potential approaches (Mo and Ching 2000; Mizoguchia et al. 2006).

In this paper, we report a Mg *K*-edge XANES study of a large selection of minerals and synthetic silicate glasses belonging to the systems $\text{Na}_2\text{O}-\text{K}_2\text{O}-\text{MgO}-\text{Al}_2\text{O}_3-\text{SiO}_2$ and $\text{X}_2\text{O}-\text{MgO}-\text{SiO}_2$ ($\text{X} = \text{Li}, \text{Na}, \text{K}, \text{Rb}$ and Cs). To ensure the interpretation of the Mg *K*-edge spectra of glasses, the selected minerals present a wide variety of Mg environments, with coordination number ranging from 4 to 8. Relationships between pertinent structural parameters and the variations observed between XANES spectra of a selection of minerals are derived from first-principles full-potential calculations, based on density functional theory. The method uses plane-wave basis set and treats the core-hole effects within a supercell.

The paper is organized as follows. The section “**Experimental and calculation methods**” includes a description of the crystalline and glass samples. The section “**Results and discussion**” is divided in two main parts. The first one is concerned with the reference minerals. The experimental spectra are compared with calculations, with a special attention given to the two-site Mg compounds. In the second part, the experimental spectra of glasses are presented and analyzed in the light of the results obtained for the reference mineral spectra. Conclusions of this work are summarized in last section.

Experimental and calculation methods

Samples

Ten natural and synthetic minerals bearing Mg in various environments are studied. Magnesium atoms occupy either one or two non equivalent crystallographic sites, with eight-fold (^{81}Mg), six-fold (^{61}Mg), five-fold (^{51}Mg) and four-fold (^{41}Mg) coordination. Minerals with a single Mg site are pyrope ($^{81}\text{Mg}_3\text{Al}_2\text{Si}_3\text{O}_{12}$, Arendal, Norway), cordierite ($^{61}\text{Mg}_2\text{Al}_4\text{Si}_5\text{O}_{18}$, Bamble, Norway), monticellite ($\text{Ca}^{61}\text{MgSiO}_4$, Mt Vesuvius, Italy), diopside ($\text{Ca}^{61}\text{MgSi}_2\text{O}_6$, Skardu, Pakistan), grandidierite (Farges 2001) ($^{51}\text{Mg,FeAl}_3\text{BSiO}_9$, Ampamatoa, Madagascar), and spinel ($^{41}\text{MgAl}_2\text{O}_4$,

Beronono, Madagascar). Minerals with two Mg sites are forsterite ($^{61}\text{Mg}_2\text{SiO}_4$, San Carlos, USA), enstatite ($^{61}\text{Mg}_2\text{Si}_2\text{O}_6$, Sagae, Pakistan), talc ($^{61}\text{Mg}_3\text{Si}_4\text{O}_{10}(\text{OH})_2$, Luzenac Ariège, France), and farringtonite ($^{55-61}\text{Mg}_3\text{P}_2\text{O}_8$, synthetic (Brunet and Vielzeuf 1996)). The model compound structures have been checked by X-ray diffraction using a X'PERT PRO MPD, Co K_α radiation and 2θ from 5° up to 110° . Table 1 gives the chemical compositions of the minerals, as determined from microprobe analysis carried out at the Camparis analytical facility of the Universities of Paris VI and VII.

Glass samples were prepared from powdered oxides and carbonates. The starting materials (SiO_2 , MgCO_3 , Li_2CO_3 , Na_2CO_3 , K_2CO_3 , Rb_2CO_3 and Cs_2CO_3) were dried overnight, weighted, mixed in an agate mortar and placed in a platinum crucible. The crucible was placed in a high temperature furnace Carbolite HTF 1700 and heated up to 600°C in 30 min. Temperature was held to 600°C for 1 h to start the decarbonation of the mixture. The temperature was elevated again up to $1,550^\circ\text{C}$ and maintained at this temperature for 1 h to obtain a homogeneous liquid. The bottom of the crucible was then fastly poured into water to quench the silicate melt into a glass. All glass samples obtained were transparent and free of crystallites determined by optical microscopic observation. Glass samples with varying NBO/T (non bridging oxygen by tetrahedron) and cation modifier were synthesized. Samples are labeled XMS2 and XMS3 (for $\text{X}_2\text{O}-\text{MgO}-2\text{SiO}_2$ and $\text{X}_2\text{O}-\text{MgO}-3\text{SiO}_2$ respectively) where X = Li, Na, K, Rb or Cs. XMS2 samples have a NBO/T = 2 while NBO/T, for XMS3 samples, is equal to 1.33, considering Mg as a network modifier for the NBO/T calculations (Mysen and Richet 2005). Moreover, three alumino-silicate glasses in the system $\text{SiO}_2-\text{Al}_2\text{O}_3-\text{MgO}-\text{Na}_2\text{O}-\text{K}_2\text{O}$ were synthesized with variable values of aluminium saturation index (ASI). The ASI characterizes the relative proportion of aluminium and alkali network modifier and is calculated using the formula, $\text{ASI} = \text{mol}\% \text{Al}_2\text{O}_3 / (\text{mol}\% \text{Na}_2\text{O} + \text{mol}\% \text{K}_2\text{O})$.

The alumino-silicate glasses of this study present three distinct values of (ASI): 0.6, 1.0 and 1.2. When $\text{ASI} < 1$, the peralkaline glass contains more alkali ions than needed to charge-balance the AlO_4^- charge. The proportions of Al and alkali ions are equal for $\text{ASI} = 1$, and when $\text{ASI} > 1$, aluminium is more abundant than alkali ions. The extra AlO_4^- charges may be charge-balanced by Mg. Therefore, some structural and electronic changes are expected that could be probed at the Mg K-edge. All samples were analyzed using a microbeam electron microprobe. The Li-bearing glasses were analyzed at the CEA (Commissariat à l'Énergie Atomique) of Saclay. The other samples were analyzed at the Camparis analytical facility of the Universities of Paris VI and VII. The column conditions for the Na- and K-bearing glasses on a CAMECA SX 100 were set to 30 kV, 4 nA and samples were analyzed with a defocused beam during 5 s in order to increase the probed volume and to minimize eventual volatilization of alkalis. Rb-, Cs-bearing glasses and natural minerals were analyzed on a CAMECA SX 50 with the column conditions set to 15 kV, 10 nA and a counting time of 5 s per points. X-ray intensities were corrected for dead time background and matrix effects using the PAP routine (Pouchou and Pichoir 1984). The chemical compositions averaged over 10 points are presented in Table 2.

X-ray absorption measurements

Mg K-edge XANES spectra were collected on the LUCIA beamline of the SOLEIL facility (Flank et al. 2006), while located at the Swiss Light Source, with an injected electron energy and current of 2.4 GeV and 350 mA, respectively. A two-crystal beryl ($10\bar{1}0$) and KTP monochromator were used as well as KB mirrors to focus the beam down to $10 \times 15 \mu\text{m}$ (vertical and horizontal). The first inflection point of the Mg K-edge of periclase MgO at 1,306.6 eV was used to calibrate the monochromator in energy. XANES spectra were recorded between 1,290 and

Table 1 Chemical composition of the minerals under study obtained from microprobe analysis

| | Ca | Mg | Al | B | Si | O | Fe | Mn | Ti | Na | Rb | Cs |
|---|-------|-------|-------|-------|-------|------|-------|-------|-------|-------|-------|-------|
| Pyrope ($\text{Mg}_3\text{Al}_2\text{Si}_3\text{O}_{12}$) | 0.324 | 1.491 | 1.997 | – | 2.986 | 12.0 | 1.167 | 0.041 | 0.002 | – | – | – |
| Cordierite ($\text{Mg}_2\text{Al}_4\text{Si}_5\text{O}_{18}$) | – | 1.687 | 4.000 | – | 4.977 | 18.0 | 0.316 | 0.003 | 0.003 | 0.051 | 0.012 | – |
| Forsterite (Mg_2SiO_4) | – | 1.796 | – | – | 1.011 | 4.0 | 0.176 | 0.003 | – | – | – | – |
| Monticellite (CaMgSiO_4) | 0.992 | 0.855 | – | – | 1.001 | 4.0 | 0.118 | 0.026 | – | – | – | – |
| Enstatite ($\text{Mg}_2\text{Si}_2\text{O}_6$) | 0.010 | 1.677 | – | – | 2.008 | 6.0 | 0.281 | – | – | 0.002 | – | – |
| Diopside ($\text{CaMgSi}_2\text{O}_6$) | 0.999 | 0.885 | 0.018 | – | 1.989 | 6.0 | 0.098 | 0.003 | – | 0.012 | – | – |
| Grandidierite ($(\text{Mg},\text{Fe})\text{Al}_3\text{BSiO}_9$) | – | 0.838 | 3.051 | 0.885 | 1.027 | 9.0 | 0.204 | – | 0.001 | – | – | – |
| Spinel (MgAl_2O_4) | – | 0.917 | 2.007 | – | – | 4.0 | 0.066 | – | – | – | 0.003 | 0.002 |

The theoretical chemical formulae are indicated in parenthesis. The chemical composition of talc has not been determined due to the impossibility to obtain a plane surface required for microprobe analysis. Farringtonite does not appear in the table since it is a synthetic sample

Table 2 Electron microprobe chemical analysis (in weight %) of silicate glasses

| | SiO ₂ | Al ₂ O ₃ | CaO | MgO | FeO | Li ₂ O | Na ₂ O | K ₂ O | Rb ₂ O | Cs ₂ O | Total |
|---------|------------------|--------------------------------|------|------|------|-------------------|-------------------|------------------|-------------------|-------------------|-------|
| LiMS2 | 63.7 | n.m. | n.d. | 20.4 | n.m. | 15.7 | n.m. | n.m. | n.m. | n.m. | 99.8 |
| LiMS3 | 72.8 | n.m. | n.d. | 15.6 | n.m. | 12.0 | n.m. | n.m. | n.m. | n.m. | 100.4 |
| NaMS2 | 55.5 | n.d. | n.d. | 16.9 | n.m. | n.m. | 27.7 | n.d. | n.m. | n.m. | 100.1 |
| NaMS3 | 63.3 | n.d. | n.d. | 13.3 | n.m. | n.m. | 22.9 | n.d. | n.m. | n.m. | 99.8 |
| KMS2 | 50.2 | n.d. | n.d. | 15.6 | n.m. | n.m. | n.d. | 33.3 | n.m. | n.m. | 99.1 |
| KMS3 | 56.6 | n.d. | n.d. | 12.0 | n.m. | n.m. | n.d. | 29.8 | n.m. | n.m. | 98.4 |
| RbMS2 | 41.1 | 0.5 | n.d. | 12.3 | n.d. | n.m. | n.d. | n.d. | 43.0 | n.d. | 96.9 |
| RbMS3 | 46.8 | 0.5 | n.d. | 9.2 | n.d. | n.m. | n.d. | n.d. | 40.8 | 0.2 | 97.5 |
| CsMS2 | 35.5 | n.d. | n.d. | 10.0 | n.d. | n.m. | n.d. | 0.1 | n.d. | 54.0 | 99.6 |
| CsMS3 | 38.8 | n.d. | n.d. | 8.4 | n.d. | n.m. | n.d. | n.d. | n.d. | 52.2 | 99.4 |
| ASI_1.2 | 71.6 | 14.8 | n.d. | 2.9 | n.d. | n.m. | 3.7 | 5.6 | n.d. | n.m. | 98.6 |
| ASI_1.0 | 71.7 | 12.9 | n.d. | 3.0 | n.d. | n.m. | 4.1 | 6.1 | n.d. | n.m. | 97.8 |
| ASI_0.6 | 71.4 | 10.9 | n.d. | 3.2 | n.d. | n.m. | 5.2 | 8.0 | n.d. | n.m. | 98.7 |

n.m. not measured; *n.d.* not detected

1,400 eV with energy steps of 0.1 eV and between 1,400 and 1,550 eV with energy steps of 0.2 eV with a counting time of 1 s per point. All samples were mounted on copper slide using glue or silver lacquer. XANES spectra were collected in the fluorescence mode with a silicon drift diode detector. To increase the signal to noise ratio, three spectra per sample were averaged together. Samples were placed perpendicular to the beam and the detector was placed at 73° of the beam to minimize as much as possible self-absorption effects. In spite of this precaution, XANES spectra of spinel, farringtonite, enstatite, forsterite and pyrope were corrected of self-absorption by using FLUO software developed by Haskel (1999). For the other model compounds and the synthetic silicate glasses, self-absorption was found to be negligible. Spectra were deadtime corrected, and normalized in absorbance using conventional methods (Winterer 1997).

XANES calculation

The method used to calculate the XANES spectra of model compounds is a self-consistent full-potential approach¹ based on the Density Functional Theory (DFT) in the Local Density Approximation (LDA): it uses a plane wave basis set, norm-conserving Troullier-Martins pseudopotentials (Troullier and Martins 1991) and periodic boundary conditions. Reciprocal-space integrations are performed using a Monkhorst-Pack *k*-point grid (Monkhorst and Pack

1976). All-electron wave function are reconstructed using the Projector Augmented Wave method (Blöchl 1994) and the cross-section is computed as a continued fraction (Taillefumier et al. 2002; Cabaret et al. 2005).

The calculations were performed on four minerals whose structures contain a single crystallographic Mg site (spinel, grandidierite, diopside and pyrope), and three minerals in which Mg is located in two distinct crystallographic sites (farringtonite, enstatite and forsterite). In the case of forsterite, farringtonite and enstatite, the theoretical Mg *K*-edge XANES spectrum is the average of the individual contributions obtained with the absorbing atom located at each non equivalent crystallographic site. Calculations were carried out from the experimental crystal structures listed in Table 3. In the case of forsterite, pyrope, enstatite, diopside and spinel, calculations were performed from theoretical chemical compositions, that do not contain any impurity or trace element. For the calculation of the Mg *K*-edge XANES spectrum of grandidierite ((Mg,Fe)Al₃BSiO₉), the presence of Fe is ignored and Mg occupies all the divalent sites.

As periodic boundary conditions are used, the core-hole-electron interaction is taken into account in a supercell approach, that permits to isolate the absorbing atom. Convergence is reached for the following size of supercells: 2 × 2 × 2 trigonal supercell for spinel (containing 112 atoms), 1 × 1 × 2 monoclinic supercell for diopside (containing 80 atoms), 1 × 1 × 1 cubic supercell for pyrope (containing 160 atoms), 2 × 1 × 2 monoclinic supercell for farringtonite (containing 104 atoms), 2 × 1 × 2 orthorhombic supercell for forsterite (containing 112 atoms), and 1 × 1 × 2 orthorhombic supercell for grandidierite and enstatite (containing 120 and 160 atoms, respectively).

¹ Calculations were performed with PARATEC (PARAllel Total Energy Code) by B. Pfrommer, D. Raczowski, A. Canning, S.G. Louie, Lawrence Berkeley National Laboratory (with contributions from F. Mauri, M. Cote, Y. Yoon, Ch. Pickard and P. Haynes). For more information see <http://www.nersc.gov/projects/paratec>.

Table 3 Crystallographic structure of minerals used in XANES calculations

| | Spinel ^a | Grandidierite ^b | Diopside ^c | Pyrope ^d | Farringtonite ^e | Forsterite ^f | Enstatite ^g |
|---------------|----------------------------------|-------------------------------------|------------------------------------|---|---|----------------------------------|--|
| Chem. formula | MgAl ₂ O ₄ | MgAl ₃ SiBO ₉ | CaMgSi ₂ O ₆ | Mg ₃ Al ₂ Si ₃ O ₁₂ | Mg ₃ (PO ₄) ₂ | Mg ₂ SiO ₄ | Mg ₂ Si ₂ O ₆ |
| Cryst. syst. | Cubic | Orthorhombic | Monoclinic | Cubic | Monoclinic | Orthorhombic | Orthorhombic |
| Space group | <i>Fd3m</i> | <i>Pbnm</i> | <i>C2/c</i> | <i>Ia3d</i> | <i>P2₁/n</i> | <i>Pbnm</i> | <i>Pbca</i> |
| a (Å) | 8.080 | 10.340 | 9.746 | 11.548 | 7.596 | 4.755 | 18.216 |
| b (Å) | | 10.980 | 8.899 | | 8.231 | 10.198 | 8.813 |
| c (Å) | | 5.750 | 5.251 | | 5.078 | 5.979 | 5.177 |
| β (°) | | | 105.63 | | 94.05 | | |
| Z | 8 | 4 | 4 | 8 | 2 | 4 | 16 |

Z is the number of formula units per cell

^a from Yamanaka and Takeuchi (1983); ^b from Stephenson and Moore (1968); ^c from Cameron et al. (1973); ^d from Hazen and Finger (1989); ^e from Nord and Kierkegaard (1968); ^f from Boström (1987); ^g from Hawthorne and Ito (1977)

Table 4 Parameterization used for the generation of the pseudopotentials

| Atom | Valence states | | | Local part |
|------|--------------------------|--------------------------|--------------------------|------------|
| Mg | 3s ^{0.1} (1.06) | 3p ⁰ (1.06) | 3d ⁰ (1.06) | <i>d</i> |
| Al | 3s ² (1.06) | 3p ⁰ (1.06) | 3d ⁰ (1.06) | <i>d</i> |
| Si | 3s ² (1.06) | 3p ^{1.3} (1.06) | 3d ^{0.2} (1.06) | <i>d</i> |
| P | 3s ² (1.06) | 3p ^{1.8} (1.06) | 3d ^{0.2} (1.06) | <i>d</i> |
| B | 2s ² (0.97) | 2p ¹ (0.97) | | <i>p</i> |
| Ca | 3s ² (0.77) | 3p ⁶ (1.06) | 3d ⁰ (0.77) | <i>d</i> |
| O | 2s ² (0.77) | 2p ⁴ (0.77) | | <i>p</i> |

The core radii of the valence states are indicated in parentheses in Å

The norm-conserving pseudopotentials were generated in the Kleinman-Bylander form (Kleinman and Bylander 1982) using the parameterization given in Table 4. The pseudopotential of the absorbing atom was obtained by considering only one 1s electron on the magnesium electronic configuration. The Mg pseudopotential (with and without the 1s core-hole) includes non-linear core-corrections. The self-consistent potential was obtained in the LDA as formulated by Ceperley and Alder (1980) with a 60 Ry energy cut-off for the plane-wave expansion, and a 2 × 2 × 2 *k*-point grid for spinel, grandidierite, diopside, pyrope, farringtonite and forsterite and a 1 × 1 × 1 *k*-point grid for enstatite. The cross-section was calculated using a 4 × 4 × 4 *k*-point grid for spinel, grandidierite, diopside and pyrope and a 3 × 3 × 3 *k*-point grid for farringtonite, forsterite and enstatite. The continued fraction is calculated with a constant broadening parameter of 0.5 eV for all the model compounds. In order to properly align all the theoretical XANES spectra between each other, we have used the method described by Cabaret et al. (2007). This is needed because the 1s energy as well as the conduction band edge in presence of a core-hole are both site-dependent.

Results and discussion

Minerals

Experimental XANES spectra

Normalized Mg *K*-edge XANES spectra of the ten model compounds are presented in Fig. 1. Despite the great differences observed between the experimental spectra, the edge region can be described by three main features in the energy range 1,305–1,320 eV followed by a broader and weaker peak located between 1,323 and 1,331 eV. Labels have been assigned to the features according to their energy position. The three main peaks are labeled A, B and C except for the case of forsterite and cordierite, where the main features are labeled A, A', and B since no peak is present in the energy range of the peak labeled C (1,316–1,318 eV). The broader peak at higher energy is labeled D. Four additional labels (P, A', D' and D'') are introduced in order to fully describe the edge region of the model compounds: P is assigned to the pre-edge peak visible on the spectra of grandidierite, farringtonite, enstatite, talc and pyrope, A' is referred to the low-energy shoulder of feature A of the grandidierite spectrum, D' is attributed to the extra peak located between features C and D in forsterite, cordierite, diopside and spinel spectra, and D'' designates the feature located at 1333.2 eV in the cordierite spectrum.

The experimental spectra of Fig. 1, that have been recorded in fluorescence detection mode on the recent LUCIA beam line, are in good agreement with Mg *K*-edge spectra recorded in total electron yield detection mode on other beam lines (see Ildefonse et al. (1995), Andrault et al. (1998), Li et al. (1999) and Shiono et al. (2002) for spinel; Li et al. (1999) for grandidierite; Ildefonse et al. (1995) and Li et al. (1999) for diopside; Andrault et al. (1998), Cabaret et al. (1998) and Li et al. (1999) for enstatite; Ildefonse et al. (1995), Andrault et al. (1998), Li et al. (1999) for pyrope; Wu et al. (2004) for monticellite; and Li et al.

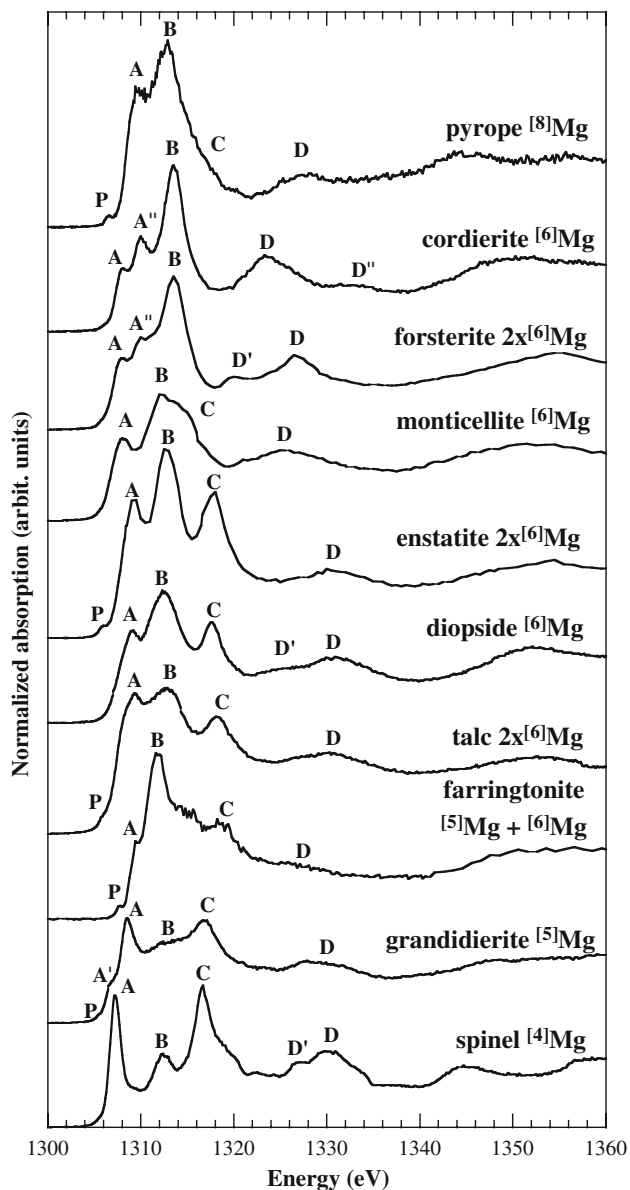


Fig. 1 Experimental Mg K-edge XANES spectra of the ten reference minerals

(1999) for talc and cordierite). Some slight discrepancies could be however noticed between our spectra and those published by Li et al. (1999). On their spectra, the pre-edge peak P is missing in the enstatite spectrum, peak A' is not present in the grandierite spectrum, peak C is clearly observed in the cordierite spectrum and is more pronounced in the pyrope one. Our forsterite Mg K-edge XANES is slightly different from that of a synthetic forsterite (Li et al. 1999; Wu et al. 2004). In particular, this latter exhibits a peak C and does not present peak D' at 1,320 eV. The absence of peak C in our forsterite Mg-K edge spectrum could be related to the presence of Fe (see Table 1). The main difference between the spectra of

forsterite and olivine Fo50, the intermediate 1:1 member of the forsterite-fayalite solid solution, as measured by Wu et al. (2004), is indeed the disappearance of peak C. The relation between the absence of peak C and the presence of Fe may be extended to the case of cordierite and pyrope. While the Mg K-edge spectrum of our Fe-bearing cordierite sample (see Table 1) does not display any feature in the energy range of peak C, the Mg K-edge spectrum of the Fe-free cordierite sample of Li et al. is characterized by a well-resolved C peak, just as mentioned above (Li et al. 1999). Similarly, peak C is more pronounced in the Mg K-edge spectrum of synthetic pyrope (Andraut et al. 1998; Li et al. 1999) than in our pyrope spectrum measured on natural Fe-bearing sample (Table 1).

Considering their overall shape, the ten spectra displayed in Fig. 1 can be categorised in three groups. A first group, composed of the spectra of spinel and grandierite, is characterized by a sharp peak A, whose intensity is equal to that of peak C, and a weak feature B. The environment of Mg is however substantially different within both crystallographic structures. While Mg is in a regular tetrahedron in the $MgAl_2O_4$ spinel structure, it occupies a distorted five-fold coordinated site within an aluminoborosilicate network in the $(Mg,Fe)Al_3BSiO_9$ grandierite structure. The geometry of the five-fold site is between distorted trigonal bipyramid and distorted tetragonal pyramid. A second group, which gathers talc, diopside and enstatite spectra, is characterized by four peaks A, B, C and D at almost the same position, peak B being the most intense. Diopside ($CaMgSi_2O_6$) and enstatite ($Mg_2Si_2O_6$) are chain silicates and talc ($Mg_3Si_4O_{10}(OH)_2$) is a layer one. In the three crystallographic structures, the Mg octahedra are edge-connected within planes located between SiO_2 planes. In the third group, composed of cordierite and forsterite, the first three major peaks, A, A' and B, have increasing intensities with energy, and peak C is absent. Cordierite ($Mg_2Al_4Si_5O_{18}$) is a framework silicate characterized by rings of corner-linked SiO_4 and AlO_4 tetrahedra. These latter are also linked by vertex to MgO_6 octahedra, which are indirectly connected to each other via edge-sharing AlO_4 and SiO_4 tetrahedra. The forsterite structure (Mg_2SiO_4), whose density is greater than that of cordierite, is an orthosilicate where Mg octahedra share edges and corners to other MgO_6 octahedra and to SiO_4 tetrahedra. Although monticellite ($CaMgSiO_4$) belongs to the olivine crystallographic group, its spectrum does not look like the one of forsterite: it does not exhibit the A' and has a broad peak B located between features A' and B of the forsterite spectrum. There are two remaining spectra, i.e. that of pyrope ($Mg_3Al_2Si_3O_{12}$), a garnet with eight-fold coordinated Mg, and farringtonite ($Mg_3P_2O_8$), a phosphate mineral with both $[^5]Mg$ and $[^6]Mg$, whose XANES spectrum is intermediate between that of enstatite and of

pyrope. From this attempt of classification of spectra according to their shape, it comes out that the Mg *K*-edge XANES spectra are controlled by several structural factors, and that a fingerprint analysis of the XANES features is not straightforward.

However, Fig. 1 shows that the first XANES feature (peak A) is shifted towards higher energies when Mg coordination number increases. That is a general trend that has been previously used as a fingerprint of Mg coordination number (Ildefonse et al. 1995; Li et al. 1999). As referred to the position of peak A of spinel (^{41}Mg), the maximum shift (2.5 eV) is observed for pyrope (^{81}Mg). For ^{61}Mg -bearing compounds, the shift of peak A ranges from 0.8 to 2.2 eV. For grandidierite (^{51}Mg), the evaluation of the shift can be done from the position of either peak A' (−0.4 eV) or peak A (1.3 eV). The energy position of peak A as well as the shift (called Δ_{exp}) are reported in Table 5. This observation may provide a useful probe of the coordination number of Mg in glasses, gels, or poorly crystallized materials. However, considering solely the shift of peak A, it should be noticed that five-fold Mg cannot be clearly distinguished from six-fold Mg in the model compounds under study (see Fig. 1; Table 5). Similar trend of edge shift between 4 and 6 coordination

numbers of the absorbing atom has also been observed at the Si *K*-edge (Sharp et al. 1996) and at the Al *K*-edge (Ildefonse et al. 1998; Guili et al. 2000).

Since coordination number is tightly related to the mean distance $\langle d_{\text{Mg-O}} \rangle$, correlation between the energy position of peak A and $\langle d_{\text{Mg-O}} \rangle$ may be investigated. In Table 5, we report the Mg–O mean bond length and the experimental shifts Δ_{exp} and Δ'_{exp} . Our data are compared to previous results (Li et al. 1999). In this last study, Li and co-workers established a polynomial correlation between peak A position and Δ'_{exp} only because they have considered the mean energy position of peaks A' and A for cordierite and forsterite (Li et al. 1999). Moreover their Δ'_{exp} values are not in full agreement with ours (three over eight differs by 0.3 eV). Consequently, the use of such correlation function to determine the mean Mg–O distance in amorphous materials appears to be awkward.

The qualitative analysis of experimental spectra is strongly limited although the structural information on the local arrangement around Mg is contained in Mg *K*-XANES. The main structural information that could be directly extracted from the spectra is the evaluation of the Mg coordination number. The fingerprint study of the peak A position indeed permits the discrimination between

Table 5 Peak A energy position (in eV \pm 0.1) and shift (in eV) as referred to spinel for the ten minerals

| Mineral | CN | peak A | Δ_{exp} | Δ'_{exp} | Δ_{calc} | $\langle \text{Mg-O} \rangle$ | σ | QE | AV |
|---------------|-----------|--------------|-----------------------|------------------------|------------------------|-------------------------------|----------|-------|-------|
| Pyrope | 8 | 1,309.7 | 2.5 | 2.5 | 2.4 | 2.27 | 0.07 | – | – |
| Cordierite | 6 | 1,308.1 | 0.9 | 1.2 | – | 2.11 | 0.01 | 1.041 | 128.5 |
| Forsterite | 6 × 2 | 1,308.0 | 0.8 | 1.1 | 0.8 | 2.11 | 0.06 | – | – |
| | <i>M1</i> | – | – | – | 0.8 | 2.10 | 0.03 | 1.027 | 95.2 |
| | <i>M2</i> | – | – | – | 0.8 | 2.13 | 0.07 | 1.026 | 89.4 |
| Monticellite | 6 | 1,308.1 | 0.9 | – | – | 2.13 | 0.04 | 1.031 | 110.0 |
| Enstatite | 6 × 2 | 1,309.1 | 1.9 | 2.0 | 2.1 | 2.11 | 0.13 | – | – |
| | <i>M1</i> | – | – | – | 2.1 | 2.08 | 0.06 | 1.009 | 27.1 |
| | <i>M2</i> | – | – | – | 1.0 | 2.15 | 0.16 | 1.049 | 139.9 |
| Diopside | 6 | 1,309.1 | 1.9 | 1.9 | 2.1 | 2.08 | 0.03 | 1.005 | 17.4 |
| Talc | 6 × 2 | 1,309.3 | 2.1 | 1.9 | – | 2.07 | 0.01 | – | – |
| | <i>M1</i> | – | – | – | – | 2.07 | 0.01 | 1.009 | 28.6 |
| | <i>M2</i> | – | – | – | – | 2.07 | 0.01 | 1.009 | 28.6 |
| Farringtonite | 5, 6 | 1,309.2 | 2.0 | – | 1.9 | 2.08 | 0.08 | – | – |
| | 6 | – | – | – | 2.5 | 2.13 | 0.04 | 1.018 | 58.5 |
| | 5 | – | – | – | 1.9 | 2.05 | 0.10 | – | – |
| Grandidierite | 5 | 1,306.8 (A') | −0.4 | – | 0.1 | 2.04 | 0.08 | – | – |
| | | 1,308.6 (A) | 1.3 | 1.7 | 1.5 | | | | |
| Spinel | 4 | 1,307.2 | 0 | 0 | 0 | 1.92 | 0.00 | – | – |

Three evaluations of the shift are given: two experimental Δ_{exp} (from Fig. 1) and Δ'_{exp} [from a previous study (Li et al. 1999)], and one theoretical (from Fig. 2). The coordination number (CN) of Mg, the mean Mg–O distance (\AA) and the standard deviation (σ in \AA) of the Mg–O distance are also mentioned. For each two-site compound, specific lines (in italic) relative to each non-equivalent Mg site are added. For ^{61}Mg , the quadratic elongation (QE) and the angular variance (AV) are given in order to evaluate the degree of distortion of the octahedron. The structural parameters, $\langle \text{Mg-O} \rangle$, QE and AV are determined from the crystallographic structures given in Table 3 and in Hochella et al. (1979), Sharp et al. (1987) and Perdikatsis and Burzlaff (1981) for cordierite, monticellite and talc, respectively

$^{[4]}\text{Mg}$, $^{[6]}\text{Mg}$ and $^{[8]}\text{Mg}$. However, $^{[5]}\text{Mg}$ is difficult to distinguish from $^{[4]}\text{Mg}$ and $^{[6]}\text{Mg}$. Consequently, to go further on the interpretation of the XANES features, calculations appear to be necessary.

Comparison between experimental and calculated XANES spectra

Computed XANES spectra for spinel, granddierite, farringtonite, diopside, enstatite, forsterite and pyrope are presented in Fig. 2. An overall good agreement is obtained between experimental and calculated spectra. This agreement is especially good in the case of spinel and

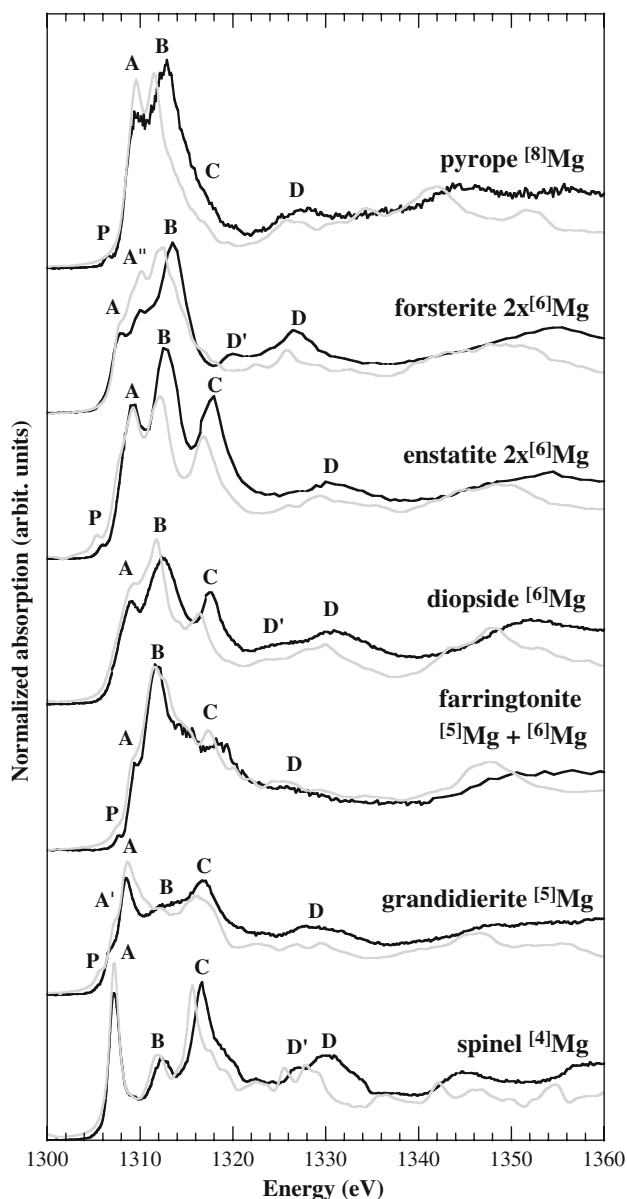


Fig. 2 Comparison between calculated (grey line) and experimental (black line) Mg K-edge XANES spectra for seven over the ten reference minerals considered in this study

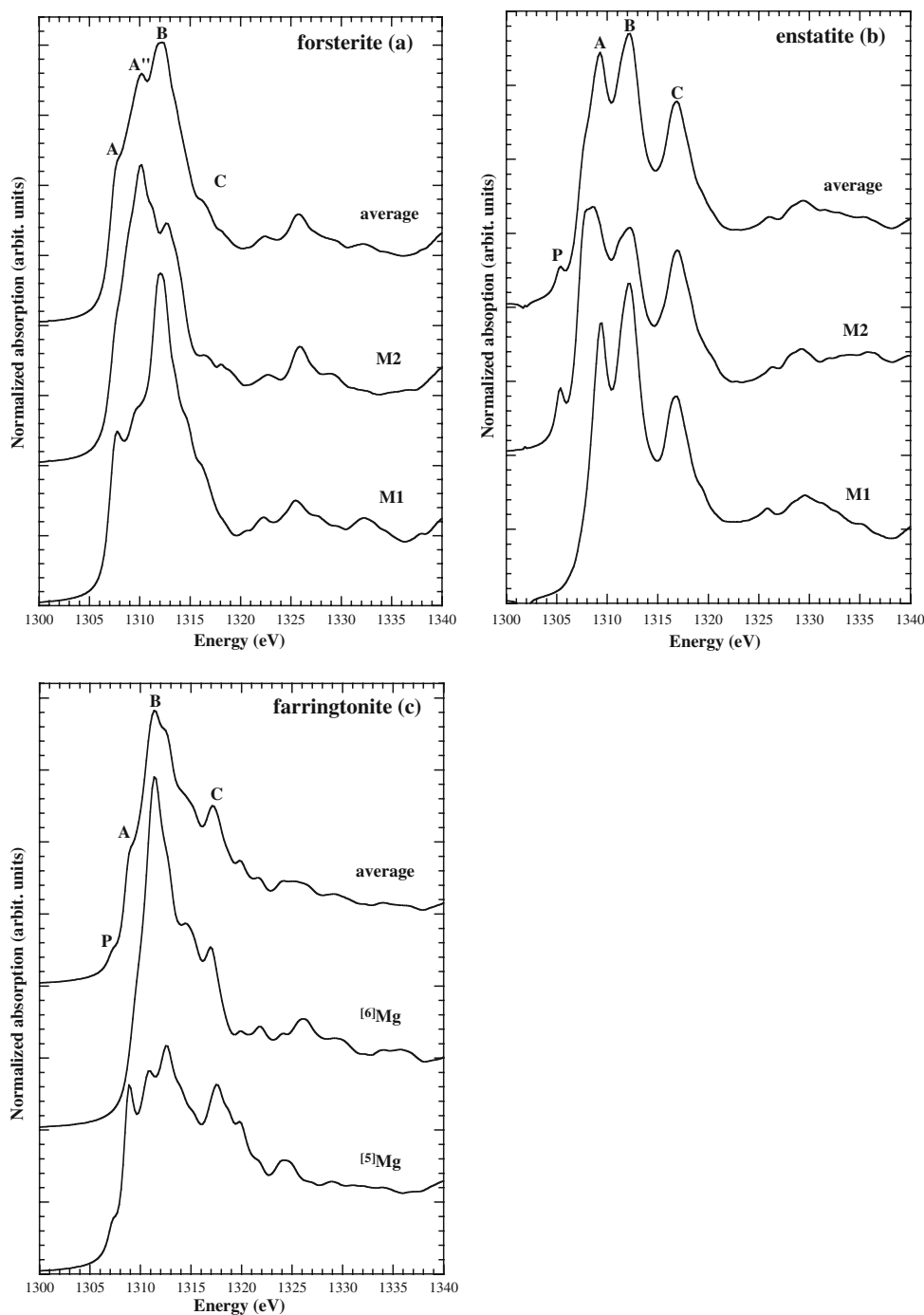
farringtonite. All the features of the experimental spectra (even the pre-edge peak P) are reproduced by the plane-wave DFT-LDA calculations. Since the method does not calculate absolute energies, all the calculated spectra are energy-rescaled by taking into account the 1s-core shift which is site-dependent (see “XANES calculation”). This rescaling is achieved by applying the same value to all the calculated spectra, in such a way that the calculated feature A of spinel coincides with the experimental one. It can be noticed that the theoretical shift of the A feature (Δ_{calc}) is in good agreement with the shift observed experimentally (see Table 5). Nevertheless, in all cases, peaks B, C and D are at too low energies as compared with experiment. Such mismatch between theory and experiment is currently observed within DFT-LDA framework, which is known to underestimate conduction band energies [see for instance the Al K-edge in $\alpha\text{-Al}_2\text{O}_3$ (Cabaret et al. 2005), the O K-edge in GeO_2 polymorphs (Cabaret et al. 2007) and $\alpha\text{-quartz}$ (Taillefumier et al. 2002), the Mg K-edge in MgO and in spinel (Mo and Ching 2000)]. Indeed our method neglects photo-electron self-energy effects, which give rise, notably, to an energy dependent shift. The agreement between the experimental and calculated positions of high-energy features could be improved by performing additional GW self-energy calculation using a many-pole model (Kas et al. 2007).

Two Mg-site spectra

In the case of forsterite, enstatite and farringtonite, since Mg occupies two non equivalent crystallographic sites, the theoretical spectrum is the average of two individual contributions, weighted according to the Mg site multiplicity. In forsterite and enstatite, Mg is located in two six-fold sites, called M1 and M2, with identical multiplicities. In farringtonite, Mg is located in five-fold and six-fold coordinated sites, with a multiplicity ratio of 2:1. The individual spectra, together with the weighted averaged spectrum, are plotted in Fig. 3.

In the case of forsterite (Fig. 3a), the M1 and M2 sites display distinct calculated Mg K-edge absorption spectra, with strong differences in the relative intensities of features A, A', B and C. The M1 spectrum is found to be similar to the one of cordierite (Fig. 1). Although the cordierite and forsterite crystallographic structures are substantially different, some similarities in the environment of the forsterite M1 site and of the cordierite Mg site may be put forward to justify their common Mg K-edge shape. Indeed the MgO_6 octahedra in both environments share edges with six polyhedra and corners with six other polyhedra: the M1 site in forsterite is edge-connected to four MgO_6 and two SiO_4 , and the MgO_6 octahedron in cordierite is linked by edge to six SiO_4 . The forsterite M2 site differs from the M1 site in

Fig. 3 Individual calculated Mg *K*-edge XANES spectra and their weighted average for forsterite (a), enstatite (b) and farringtonite (c)



such a way that it shares edge with only two MgO_6 and one SiO_4 . Moreover Fig. 3a contains the following information. Feature B is essentially due to Mg in M1 site, while the A'' peak is a fingerprint of Mg located in the M2 site. The A feature results from contributions with similar intensity of both M1 and M2 spectra (a well-resolved peak and a shoulder of peak A'', respectively). It is then possible to define a Δ_{calc} value for each Mg site and this value is identical for M1 and M2 sites of forsterite (see Table 5). It should be noticed that the calculated spectrum of forsterite

presents a C peak, mainly originating from the M1 site contribution, whereas it does not exist in the forsterite experimental spectrum (see “[Experimental XANES spectra](#)”). The presence of peak C in the forsterite calculated spectrum corroborates the fact that it may be related to the absence of Fe in the Mg crystallographic site. Similarly, in the case of pyrope (Fig. 2) one can also notice that a weak peak C is reproduced by the calculation that is performed on a *pure* pyrope phase. Nevertheless, further calculations including iron impurities are required in order to clearly

evidence such correlation. In the case of enstatite (Fig. 3b), the M1 and M2 individual spectra both exhibit three main features, that contribute to the A, B and C of the total spectrum in a similar way. Some differences between M1 and M2 are however noticeable. First, the three features A, B and C are broader in the M2 spectrum than in the M1 spectrum. Second, the relative intensity of A and B are reverse between both M1 and M2 spectrum. Third, the first peak of the M2 contribution, beside being broader, is at lower energy as compared to peak A in the M1 contribution. The corresponding site-dependent Δ_{calc} values are indicated in Table 5. Fourth, the last significant difference between both individual spectra lies in the presence of the pre-edge peak P only in the M2 spectrum. This last observation is contradictory with full multiple scattering calculation of the Mg *K*-edge in the same structure (Cabaret et al. 1998). Indeed in Cabaret et al. (1998), the pre-edge peak is reproduced on both M1 and M2 individual spectra. Since pre-edge features are known to be strongly sensitive to details of the electronic structure around the absorber, the presence of peak P in the M1 spectrum of Cabaret et al. (1998) then appears to be a theoretical artefact due to the use a non self-consistent *muffin-tin* potential, with a core-hole modelled in the $Z + 1$ approximation. The origin of the pre-edge peak will be discussed at the end of the subsection.

In the case of farringtonite (Fig. 3c), the individual computed spectra exhibit very different shapes. At least to a certain extent, the ^{51}Mg spectrum looks like the grandierite spectrum, where Mg is in five-fold coordination too, and the ^{61}Mg is quite close to the forsterite M2 spectrum. Similarly to the M2 site of forsterite, the six-fold Mg site of farringtonite is connected by edge to quite few polyhedra (2 MgO_5 only). The ^{61}Mg individual spectrum mainly contributes to the B and C features. On the contrary peak A is essentially due to the ^{51}Mg individual contribution, with a Δ_{calc} value equal to the 1.9 eV value of the resulting spectrum (see Table 5). For the ^{61}Mg contribution, the Δ_{calc} is found to be greater (2.5 eV); it is determined from the position of the shoulder observed in the edge jump at 1,309.7 eV. The pre-edge could appear as a fingerprint of five-fold Mg since it originates from the ^{51}Mg individual spectrum.

Relation between peak A position and distortion of the MgO_6 octahedron

As seen before, the coordinence of the absorbing atoms affects the position of the first main peak (A). Peak A moves to higher energy as the coordination number of Mg increases. The calculations permit the determination of the site-dependent Δ values in the case of two-Mg site compounds. Table 5 shows that the variation of position of peak A is about 1.7 eV (Δ_{calc} ranges from 0.8 eV for

forsterite to 2.5 eV for farringtonite). However the position of peak A also varies within the series of six-fold coordinated Mg minerals (see Δ values in Table 5). The Mg–O mean distance is thus not a fully relevant structural parameter to be correlated to the energy position of peak A. The shift of peak A for six-fold coordinated Mg minerals may be related to the distortion of the MgO_6 octahedron, which varies strongly among the investigated references. As established by Robinson et al. a convenient and quantitative measure of the octahedron distortion is the quadratic elongation, that is found to be linearly correlated to the angular variance (Robinson et al. 1971). The quadratic elongation (QE), which is dimensionless, and the angular variance (AV) are given by:

$$\text{QE} = \frac{1}{6} \sum_{i=1}^6 \left(\frac{l_i}{l_0} \right)^2,$$

$$\text{AV} = \frac{1}{11} \sum_{i=1}^{12} (\theta_i - 90^\circ)^2,$$

where l_i corresponds to the Mg–O distance within the octahedron, l_0 is the Mg–O distance in an octahedron with O_h symmetry whose volume is equal to that of the distorted octahedron, and where θ_i is the octahedral angle. According to the values of QE and AV indicated in Table 5, the less and the most distorted octahedra in the selected compounds are M1 site of diopside and M2 site of enstatite, respectively.

In Fig. 4, the Δ shift representing the peak A position referred to that of spinel is plotted as a function of QE. Two

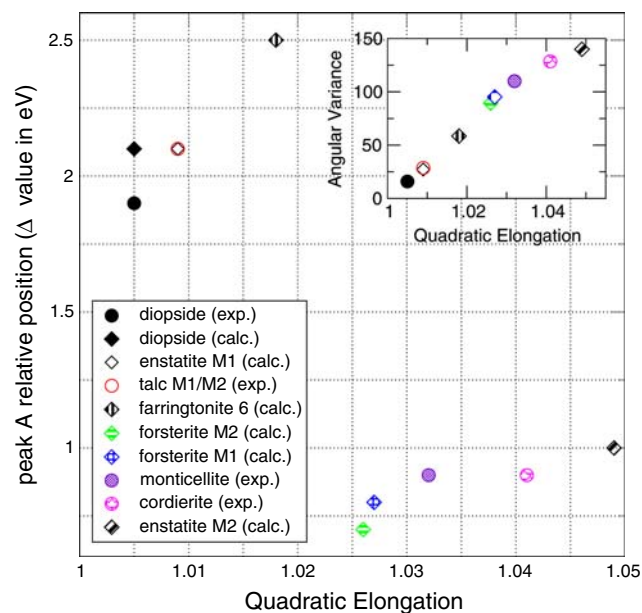


Fig. 4 Peak A position (as referred to spinel) as a function of the quadratic elongation of the MgO_6 octahedron. The inset shows the fairly linear correlation between the quadratic elongation and the angular variance as suggested by Robinson et al. (1971)

sets of data are noticeable, corresponding to $\Delta \simeq 2$ eV and $\Delta \simeq 1$ eV. The data point relative to the six-fold Mg site of farringtonite is not exactly within the first set. This may come from the fact that farringtonite is a phosphate while all the other minerals are silicates (Figure 1 does show that the whole spectrum of farringtonite is shifted to higher energy as compared to the other spectra). Figure 4 exhibits a general trend that is a $\simeq 1$ eV shift of peak A towards lower energy as the distortion of octahedron increases. An EXAFS analysis performed at the Mg *K*-edge within the pyrope-grossular garnet system reveals an increase of the Mg coordination sphere distortion as the position of peak A decreases (Quartieri et al. 2008).

At the ^{61}Al *K*-edge in minerals, the same trend can be observed from the data presented in Ildefonse et al. (1998). The Mg *K*-edge spectra of diopside crystal and glass with same composition are compared by Ildefonse et al. (1995). The glass spectrum arises at lower energy than the crystal one (1 eV). The authors conclude that Mg is five-fold coordinated in the glassy state. In the light of Fig. 4, the shift between crystal and glass spectra could be also interpreted as an increase of distortion within the octahedron.

Pre-edge

A pre-edge is present in the Mg *K*-edge experimental spectra of grandierite (^{51}Mg), farringtonite (^{51}Mg and ^{61}Mg), talc (^{61}Mg), enstatite (^{61}Mg) and pyrope (^{81}Mg). Thanks to the calculations, it was found that the pre-edge of farringtonite and enstatite originates in the individual contributions of the ^{51}Mg site and M2 site, respectively. Since pre-edge arises in spectra where Mg is five-fold coordinated, six-fold coordinated or eight-fold coordinated to oxygen, the Mg coordination number is not a relevant parameter to predict its existence. On the other hand, the asymmetric environment of Mg seems to be tightly involved in the presence of pre-edge. Intense calculated pre-edge peaks are obtained in ^{51}Mg *K* edge spectra and in the case of M2 site of enstatite, which is the most distorted site among the ^{61}Mg sites selected in this study (see Table 5). With a very long Mg–O distance (2.45 Å) the enstatite M2 site presents the strongest standard deviation of distance ($\sigma = 0.16$ Å). The asymmetry of the enstatite M2 site is then closer to that of the ^{51}Mg site of farringtonite and grandierite than to that of the other ^{61}Mg sites. Cordierite which also presents important distortion of Mg site (QE = 1.041) is characterized by a weak standard deviation of Mg–O distance ($\sigma > 0.01$ Å), so that no pre-edge is visible in the Mg *K*-edge spectrum. However talc, with weak QE and weak σ , exhibits a pre-edge. Talc is the unique compound of this study with Mg bound to OH and we assume that OH may play a significant role in the origin

of the pre-edge. However, the pre-edge observed on the talc spectrum could also be due to the fact that the phyllosilicate structure is oriented. In the case of pyrope, the calculated pre-edge is weaker than the experimental one. The Mg site is characterized by two groups of four equal distances which are rather different (i.e. 2.20 and 2.34 Å), that could be at the origin of the calculated pre-edge. The experimental spectra of pyrope shown in Ildefonse et al. (1995), Andrault et al. (1998), Li et al. (1999) and Quartieri et al. (2008) do not exhibit a well-defined pre-edge. In our pyrope sample, the total amount of Mg atoms does not exceed 1.5 instead of 3 in the theoretical chemical composition. In addition, the sample contains a non-negligible quantity of iron, whose 3*d* empty orbitals could be virtually involved in the Mg *K* pre-edge.

Unlike the *K* pre-edge of 3*d* elements in metal oxides, the origin of the *K* pre-edge of low-*Z* cation such as Mg or Al is not much discussed in the literature. In the case of 3*d* elements, three kinds of electronic transitions are used to describe the pre-edge features, as recently explained by de Groot (2007): (1) electric quadrupole transitions, $1s \rightarrow 3d$; (2) non-local electric dipole transition, $1s \rightarrow p$ where the empty *p* of absorbing atom are hybridized with the 3*d* states of the nearest metal neighbours via the 2*p* states of oxygen; (3) local electric dipole transition, $1s \rightarrow p$ where the empty *p* of the absorbing atom are hybridized with the empty 3*d* of the absorbing atom. In this latter, the *p*–*d* mixing is possible only if the absorbing atom site is not centrosymmetric. Our calculations, which are performed in the electric dipole approximation, reproduce the pre-edge peak. Therefore, it is due to transitions from 1*s* to *p* empty Mg states. Obviously, the role played by 3*d* empty states is not as important as it is in the case of 3*d* elements. In the Mg *K*-pre-edge, the 3*s* Mg states could also be involved in the pre-edge. The formal charge of Mg being +2, the 3*s* states are empty and may contribute as an important part to the bottom of the conduction band. For non-centrosymmetric Mg site (that is not the case only for the M1 site of forsterite and for the six-fold Mg site of farringtonite), *p*–*s* and *p*–*d* mixing are allowed. However the identification of non-local effects as point (2) or local effects as point (3), and their connection to the site asymmetry mentioned above, would require precise calculations of local density of states performed on supercells including the Mg 1*s* core-hole, and such calculations are beyond the scope of this paper.

Glasses

Alumino-silicate glasses

The Mg *K*-edge absorption spectra of the three alumino-silicate glasses are shown in Fig. 5. The three spectra are

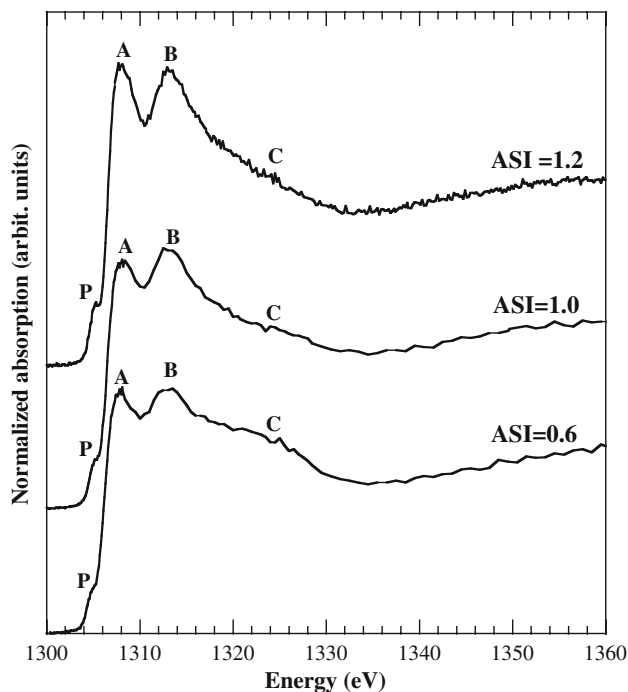


Fig. 5 Experimental Mg *K*-edge XANES spectra of the synthetic aluminosilicate glasses with different aluminium saturation index (ASI)

Table 6 Feature A position and shift (as referred to spinel) of the Mg *K*-edge spectra of the studied glasses

| Glasses | peak A (in eV \pm 0.1 eV) | Δ (eV) |
|-------------|-----------------------------|---------------|
| ASI_1.2 | 1,308.0 | +0.8 |
| ASI_1.0 | 1,308.0 | +0.8 |
| ASI_0.6 | 1,307.9 | +0.7 |
| LiMS2/LiMS3 | 1,308.5/1,308.2 | +1.3/+1.0 |
| NaMS2/NaMS3 | 1,308.1/1,307.9 | +0.9/+0.7 |
| KMS2/KMS3 | 1,307.3/1,307.5 | +0.1/+0.3 |
| RbMS2/RbMS3 | 1,307.1/1,307.2 | -0.1/+0.0 |
| CsMS2/CsMS3 | 1,307.0/1,306.9 | -0.2/-0.3 |

characterized by one pre-edge peak P and two well-defined resonances A and B, followed by one broad feature C. The positions of the four features remain constant as the index of aluminium saturation (ASI) varies. Peak A arises at $1,308 \pm 0.1$ eV yielding a shift $\Delta = 0.8$ eV as referred to peak A of spinel (see Table 6). According to the study of the minerals, this value of Δ suggests that Mg is either six-fold coordinated to oxygen atoms within a rather strongly distorted octahedron (as shown in Fig. 4) or five-fold coordinated to oxygen atoms. However the occurrence of ^{44}Mg cannot be excluded. On the contrary the presence of ^{81}Mg is almost improbable. In aluminosilicate glasses belonging to the system $\text{CaMgSi}_2\text{O}_6\text{-NaAlSi}_3\text{O}_8$, the Mg *K*-edge spectra also exhibit three main features, and the

energy position of peak A coincides with $\Delta \simeq 1$ eV, meaning that Mg would be mainly six-fold coordinated to oxygen in a distorted octahedron, coexisting with ^{51}Mg (and eventually with ^{44}Mg) (Li et al. 1999). The difference between shifts could be related to various ^{44}Mg , ^{51}Mg and ^{61}Mg proportions. Very recently, neutron and X-ray diffraction and reverse Monte Carlo modeling have revealed in the $\text{MgO-Al}_2\text{O}_3\text{-SiO}_2$ glass system the coexistence of ^{51}Mg and ^{61}Mg (in a lesser proportion) (Guignard and Cormier 2008). The presence of pre-edge in the spectra of Fig. 5 would signify that the local environment of Mg is highly asymmetric in good agreement with the previous interpretations of Mg coordination number. All these results are in perfect agreement with recent molecular dynamics simulations of complex aluminosilicate glasses that prevail Mg in 5-fold coordination (Guillot and Sator 2007).

Peak B arises at around 1,313 eV, as in cordierite, forsterite, talc and pyrope Mg *K*-edge spectra, but this spectral particularity is difficult to connect to an eventual common structural feature. Peak C appears around 1,324 eV that is 6–7 eV higher than in mineral spectra. On the contrary in Mg *K*-edge of $\text{CaMgSi}_2\text{O}_6\text{-NaAlSi}_3\text{O}_8$ glasses (Li et al. 1999), peak C is located around 8 eV above peak A as in minerals. Therefore, the unexpected position of peak C in spectra of Fig. 5 could be associated to the glass composition specificity, i.e. the presence of potassium atoms. Following the Natoli's rule (Natoli 1984), stating that the energy range between two XANES features is reverse-proportional to the characteristic interatomic distance squared ($ER^2 = \text{cst}$), the assignment of peak C to the presence of K in our glasses and to Ca in glasses of Li et al. makes sense (Li et al. 1999). Indeed potassium atoms, with large atomic radius, generate Mg–K distances greater than Mg–Ca ones.

Unlike the energy positions, the relative intensities of the XANES features are sensitive to the ASI. As ASI increases, the K proportion decreases (see Table 2) and so does the intensity of feature C, corroborating the assignment established above. Besides, when ASI increases, features A and B become more intense, and pre-edge peak P is better resolved. Such modifications imply structural atomic rearrangements around Mg that depend on the ratio Al/alkali, and that are not concerned with the coordination number of Mg. But such information is hardly extractable from the spectra without robust simulations.

XMS2 and XMS3 glasses

The experimental Mg *K*-edge XANES spectra of the XMS2 and XMS3 Mg-bearing silicate glasses are shown in Fig. 6a, b, respectively. The spectra are characterized by three main peaks, labeled A, B and C, and a pre-edge

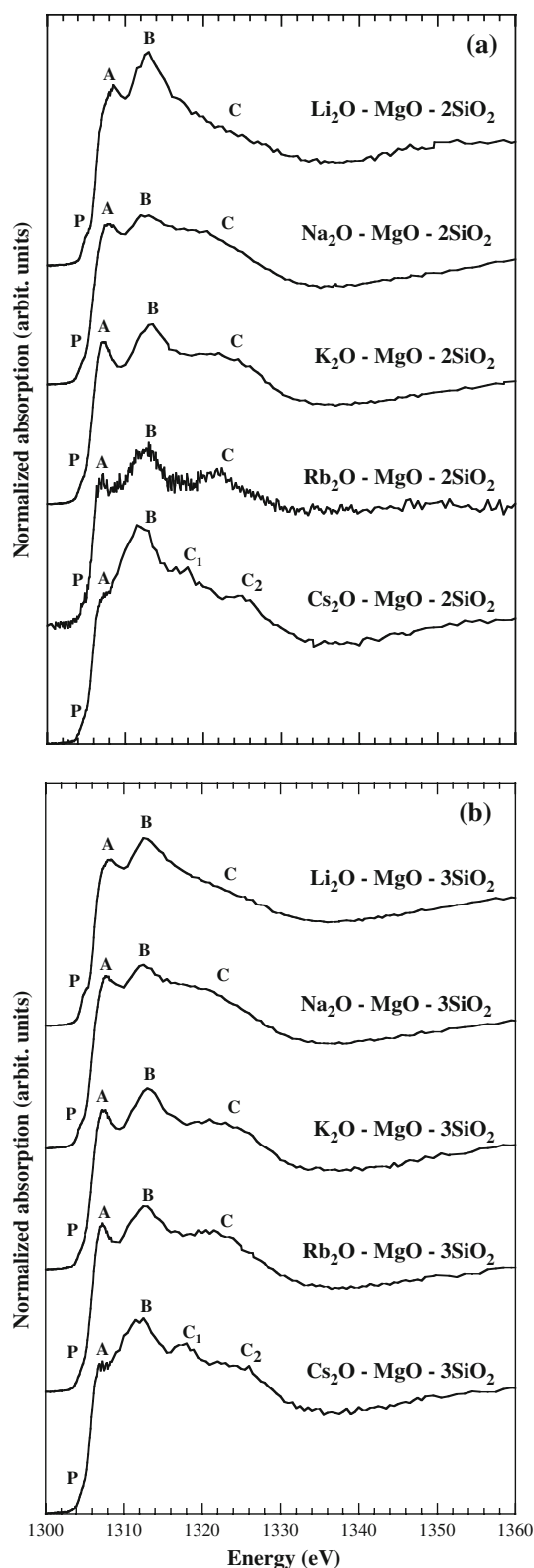


Fig. 6 Experimental Mg *K*-edge XANES spectra of the synthetic XMS2 (a) and XMS3 (b) glasses where X = Li, Na, K, Rb and Cs

feature P. Features A and B are well defined. In contrast, C is a broad feature which is scarcely observable for

Li-bearing glasses, and which is clearly split into two components C_1 and C_2 in the case of Cs-bearing glasses.

The fundamental structural difference between both XMS2 and XMS3 series is concerned with the degree of polymerization of the silicate network. Indeed the XMS2 and XMS3 glasses are characterized by $NBO/T = 2$ and $NBO/T = 1.33$, respectively. A qualitative comparison between XMS2 and XMS3 XANES spectra for the same alkali network modifier X does not evidence any significant changes in the relative intensities and the energy position of the features. This behaviour is confirmed by the position of the peak A of a NMS10 glass (spectrum not shown) which is located at 1,307.8 eV. Thus the Mg *K*-edge spectra are not sensitive to the variation of the silicate network polymerization suggesting that the Mg atomic environment is not affected by the change of polymerization of the silicate network in XMS α glasses ($\alpha = 2$ or 3). The effect of polymerization is however difficult to predict. In the system CaO–SiO₂–Al₂O₃ with NBO/T varying between 0 and 2 (Neuvillie et al. 2004) a shift (between 0.5 and 0.8 eV roughly) of the first peak of XANES spectra of glasses measured at the Ca *K*-edge spectra is observed. No shift is observed at the Al *K*-edge for the same glass compositions. In contrast, in the system Na₂O–CaO–Al₂O₃–SiO₂, no shift is observed at the Ca *K*-edge as NBO/T varies from 0.2 to 1.33. However, the edge of the Na *K*-edge XANES spectra shifts (Cormier and Neuvillie 2004). In more simple glass compositions (Na₂O–2SiO₂, Na₂O–3SiO₂, Na₂O–4SiO₂) no shift is observed at the Na *K*-edge for glasses (de Wispelaere et al. 2004). These results suggest that the shift of the first peak of XANES spectra at the *K*-edge of modifier cation strongly depends of the glass composition. No general trend can be drawn here. At the Si *K*-edge, a shift of the main peak towards the lower energy is observed as a function of the increase of depolymerization for different model compounds (Li et al. 1995). The same observations can be done for glasses in the system Na₂O–SiO₂ where the NBO/T varies from 0 up to 1.33 (Henderson 1995).

In contrast, changing the alkali ion substantially influences the XANES spectral shape. The energy positions of XANES features, as well as their relative intensities, depend on the nature of the alkali ion. Peak A is shifted towards lower energy when the alkali atomic number increases: for Li-bearing glasses, the shift of peak A (still referred to the case of spinel) is greater or equal to 1 eV, while for Cs it becomes negative ($\Delta \simeq -0.2$ eV), as reported in Table 6. Comparing the Δ values of the glasses with those of minerals (Table 5), Mg would mainly be in distorted six-fold or five-fold coordination in Li- and Na-bearing glasses, as in the aluminosilicate ASI glasses, whereas a four-fold coordination is preferred in the case of K-, Rb- and Cs-bearing glasses. The occurrence of [⁴Mg in

the potassium bearing glass is in good agreement with a recent NMR study on glasses in the same system (Shimoda et al. 2007). Similar effects have been observed for Ni- (Galoisy and Calas 1993), Ti-bearing glasses (Dingwell et al. 1994), and Fe-bearing glasses (Jackson et al. 2005). A distribution of Mg coordination number cannot be however excluded in Na- and Li-bearing glasses and is even highly probable as was observed by NMR spectroscopy for glasses in the system $\text{Na}_2\text{O}-\text{MgO}-\text{SiO}_2$ (Fiske and Stebbins 1994). The presence of a pre-edge in each spectrum also suggests a disorder within the Mg coordination sphere, that can be translated into an asymmetry in the mean environment of Mg. The existence of a distribution of Mg sites (4 + 5) is close to that found in Fe^{2+} -bearing glasses [cf. Rossano et al. (2008) and reference therein] or in Ni^{2+} -bearing glasses (Galoisy and Calas 1993) thus suggesting a similar role for the two cations in glasses. This similarity could explain the close behaviour observed for Mg^{2+} , Fe^{2+} , and Ni^{2+} in partitioning coefficients (Beattie 1994; O'Neill and Eggins 2002; Toplis 2005).

The assumption establishing a correlation between the position of peak C and the Mg–X distance ($d_{\text{Mg-X}}$) (see subsection “Alumino-silicate glasses”) seems to be corroborated by the Mg *K*-edge spectra in the XMS α system ($\alpha = 2$ or 3). Indeed Fig. 6 show that the energy position of feature C depends on the nature of the network modifier, but without following the atomic number as in the case of peak A. Peak C arises at around 1,321.5 eV for Na-bearing glasses, around 1,322 eV for Rb bearing glasses, and around 1,323.5 eV for K-bearing glasses. This latter coincides with the energy position of peak C of the alumino-silicate glasses (Fig. 5). This variation in position would mean that $d_{\text{Mg-Na}} > d_{\text{Mg-Rb}} > d_{\text{Mg-K}}$. In the case of Cs-bearing glasses, peak C is separated in two components at around 1,318 and 1,325 eV. By carrying on the argument, these two features would be the sign of two distinct Mg–Cs distances, thus two distinct Cs local environments. In the case of Li-bearing glasses, the scattering power of Li being so weak, peak C is weak and its energy position is difficult to evaluate. To conclude on this point, complementary spectroscopic studies combined with molecular dynamics calculations are needed to determine the local environment of the alkali-ions, and finally to confirm or invalidate our analysis of the Mg *K*-edge spectra.

Unlike that of peak A and C, the energy position of peak B is not much sensitive to the nature of the alkali ion (from 1,312.5 eV for CsMS3 to 1,313.3 for KMS2). The position of this peak appears to be quite a constant at the Mg *K*-edge in all the studied compounds.

The relative intensities of features A and B are also dependent on the alkali element. However, as in alumino-silicate glasses, the analysis of such variations is not straightforward and would require XANES simulations. As

in crystals, the starting point of XANES simulations in glasses is a structural model. Glass structural models can be obtained from molecular dynamics calculations. To our knowledge, very few studies have been devoted to the simulation of XANES in oxide glasses, using MD models (Levelut et al. 2001; Cabaret et al. 2001; Farges et al. 2004). Indeed the coexistence of various sites for the absorbing atom increases the computing time and complicates the spectral analysis. However the coupling of MD and robust XANES simulations is a promising approach for structural investigations in glasses.

Conclusion

X-ray absorption near-edge spectroscopy (XANES) was used at the Mg *K*-edge in order to extract information at short and medium range order around magnesium in glasses. Prior to glass analysis, Mg-bearing minerals have been studied. As Mg environment (coordination, polyhedron geometry and neighbours) varies, both relative intensities and positions of the XANES features are affected. The results presented highlight the impossibility to interpret all the observed variations by the fingerprint method.

First-principles calculation of seven crystalline compounds were performed in order to investigate the relationship between crystallographic structures and the shape of XANES spectra. The calculation method allows to reproduce with a good agreement the energy position of the first peak (labeled A) and the relative intensities of all the features including pre-edge. Although regions can be clearly assigned to Mg–O bond length for a given coordination number, the energy position of the first peak does not allow to distinguish between five-fold and six-fold coordinated Mg. The analysis of the Mg *K*-edge in crystalline compounds has shown that the shift of the feature A is the signature of a change in coordination number and/or in coordination polyhedron distortion.

Although used as reference compounds for the glass study, the results obtained on the minerals are very interesting and will be continued. For example, the good reproduction of the pre-edge feature within the electric dipole approximation shows that this feature is due to *1s* to Mg *p* empty states. Its origin should be further explored by performing local density of states calculations (for supercells including the core-hole). Such calculations would permit the identification of the states which are hybridized with Mg *p*-empty states, giving information about the covalent or ionic character of the Mg–O bond. Moreover, it would precise the role played by the asymmetry of the Mg site in the origin of the pre-edge feature. In the case of talc, the influence of OH (as Mg first neighbours) or of the oriented structure of phyllosilicate on the pre-edge feature

could be investigated. In the case of pyrope, complementary calculations are needed to clarify the possible participation of Fe states, not only in the pre-edge region, but also in the energy range of peak C. While the evidence of the connection between peak C and the absence of iron seems to be established in the case of forsterite, and from experimental observations in the case of cordierite, it is indeed less obvious in the case of pyrope.

Considering the results obtained for crystalline compound XANES spectra combined to MD and NMR results published in the literature, the magnesium coordination number has been evaluated to be mainly 5 in aluminosilicate glasses. In the XMS2 and XMS3 series, we have shown that polymerization does not affect the XANES spectra in the range investigated here. However, the type of alkali (Li, Na, K, Rb or Cs) does affect the position of the first peak A thus inducing a coordination change for the magnesium atoms. Magnesium is mainly 4-fold coordinated in Cs-, Rb- and K-glasses while its mean coordination number increases in Na- and Li-glasses being close to 5, with probably a distribution of coordination number. These results show that magnesium coordination number varies with composition thus explaining the controversies of the literature. The variation observed on peak C as a function of ASI value or alkali type has been assigned to a medium range order effect. This assumption has however to be confirmed by calculation of XANES spectra of glasses based on molecular dynamics simulations. This will allow to explore the relationship between alkali and magnesium and confirm the variation of coordination number while changing the alkali type.

Acknowledgments The authors are grateful to Sylvie Poissonnet for the recording of the microprobe analysis performed at the CEA. We are grateful to Fabrice Brunet from Ecole Normale Supérieure de Paris for providing us the farringtonite sample. The staff of Swiss Light Source (SLS) is thanked for their assistance and technical support during Mg *K*-edge measurements. The theoretical part of this work was supported by the French computational institut of Orsay (Institut du Développement et des Ressources en Informatique Scientifique) under Projects Nos. 62015 and 72015.

References

- Andraut D, Neuville DR, Flank A-M, Wang Y (1998) Cation sites in Al-rich MgSiO₃ perovskites. *Am Mineral* 83:1045–1053
- Beattie P (1994) Systematics and energetics of trace-element partitioning between olivine and silicate melts: implications for the nature of mineral/melt partitioning. *Chem Geol* 117:57–71
- Blöchl P (1994) Projector augmented-wave method. *Phys Rev B* 50:17953–17979
- Boström D (1987) Single-crystal X-ray diffraction studies of synthetic Ni-Mg olivine solid solutions. *Am Mineral* 72:965–972
- Branda F, Buri A, Caferra D, Marotta A (1983) The effect of mixing of network-modifiers on the transformation temperature of silicate glasses. *J Non-Cryst Solids* 54:193–198
- Brown GE Jr, Farges F, Calas G (1995) X-ray scattering and X-ray spectroscopy studies of silicate melts. *Rev Mineral* 32:317–410
- Brunet F, Vielzeuf D (1996) The farringtonite/Mg₃(PO₄)₂-II transformation: a new curve for pressure calibration in piston-cylinder apparatus. *Eur J Mineral* 8:221–468
- Cabaret D, Saintavitt P, Ildefonse P, Flank A-M (1998) Full multiple scattering calculations of the X-ray absorption near edge structure at the magnesium *K*-edge in pyroxene. *Am Mineral* 83:300–304
- Cabaret D, Le Grand M, Ramos A, Flank A-M, Rossano S, Galoisy L, Calas G, Ghaleb D (2001) Medium range structure in borosilicate glasses from Si *K*-edge XANES: a combined approach based on multiple scattering and molecular dynamics calculations. *J Non-Cryst Solids* 289:1–8
- Cabaret D, Gaudry E, Taillefumier M, Saintavitt F, Mauri F (2005) XANES calculation with an efficient “non muffin-tin” method: application to the angular dependence of the Al *K*-edge in corundum. *Physica Scripta T115*:131–133
- Cabaret D, Mauri F, Henderson GS (2007) Oxygen *K*-edge XANES of germanates investigated using first-principles calculations. *Phys Rev B* 75:184205
- Cameron M, Sueno S, Prewitt CT, Papike JJ (1973) High-temperature crystal chemistry of acmite, diopside, hedenbergite, jadeite, spodumene and ureyite. *Am Mineral* 58:594–618
- Ceperley DM, Alder BJ (1980) Ground state of the electron gas by a stochastic method. *Phys Rev Lett* 45:566–569
- Cormier L, Neuville DR (2004) Ca and Na environments in Na₂O-CaO-Al₂O₃-SiO₂ glasses: influence of cation mixing and cation-network interactions. *Chem Geol* 213:103–113
- Curti E (2003) Glass dissolution parameters: update for “Entsorgungsnachweis”. Technical Report NTB pp 02–21
- de Groot FMF (2007) Novel techniques and approaches to unravel the nature of X-ray absorption spectra. In: Hedman B, Pianetta P (eds) X-ray absorption fine structure—XAFS13, AIP conference proceedings, vol 882, pp 37–43
- de Wispelaere S, Cabaret D, Levelut C, Rossano S, Flank A-M, Parent P, Farges F (2004) Na-, Al-, and Si *K*-edge XANES study of sodium silicate and sodium aluminosilicate glasses: influence of the glass surface. *Chem Geol* 213:63–70
- Dingwell DB (1995) Relaxation in silicate melts: some applications. *Rev Mineral* 32:21–66
- Dingwell DB, Paris E, Seifert F, Mottana A, and Romano C (1994) X-ray absorption study of Ti-bearing silicate glasses. *Phys Chem Miner* 21:501–509
- Farges F (2001) Crystal chemistry of iron in natural grandidierites: an X-ray absorption fine-structure spectroscopy study. *Phys Chem Miner* 28:619–629
- Farges F, Lefrère Y, Rossano S, Berthereau A, Calas G, Brown GE Jr (2004) The effect of redox state on the local structural environment of iron in silicate glasses: a molecular dynamics, combined XAFS spectroscopy, and bond valence study. *J Non-Cryst Solids* 344:176–188
- Fiske PS, Stebbins JF (1994) The structural role of Mg in silicate liquids: a high-temperature ²⁵Mg, ²³Na and ²⁹Si NMR study. *Am Mineral* 79:848–861
- Flank A-M, Cauchon G, Lagarde P, Bac S, Janousch M, Wetter R, Dubuisson J-M, Idri M, Langlois F, Moreno T, Vantelon D (2006) LUCIA, a microfocus soft XAS beamline. *Nucl Instr Meth B* 246:269–274
- Galoisy L, Calas G (1993) Structural environment of nickel in silicate glass/melt systems: Part 1. spectroscopic determination of coordination states. *Geochim Cosmochim Acta* 57:3613–3626
- George AM, Stebbins JF (1998) Structure and dynamics of magnesium in silicate melts: a high-temperature ²⁵Mg NMR study. *Am Mineral* 83:1022–1029

- Guignard M, Cormier L (2008) Environments of Mg and Al in MgO-Al₂O₃-SiO₂ glasses: a study coupling neutron and X-ray diffraction and reverse monte carlo modeling. *Chem Geol* (in press)
- Guili G, Pratesi G, Corazza M, Cipriani C (2000) Aluminium coordination in tektites: a XANES study. *Am Mineral* 85: 1172–1174
- Guillot B, Sator N (2007) A computer simulation study of natural silicate melts. Part I : low pressure properties. *Geochim Cosmochim Acta* 71:1249–1265
- Haskel D (1999) FLUO package. <http://www.aps.anl.gov/xfd/people/haskel/flu.html>
- Hawthorne RM, Ito J (1977) Synthesis and crystal-structure refinement of transition-metal orthopyroxenes I: orthoenstatite and (Mg, Mn, Co) orthopyroxene. *Can Mineral* 15:321–338
- Hazen RM, Finger LW (1989) High-pressure crystal chemistry of andradite and pyrope: revised procedures for high-pressure diffraction experiments. *Am Mineral* 74:352–359
- Henderson GS (1995) A Si *K*-edge EXAFS/XANES study of sodium silicate glasses. *J Non-Cryst Solids* 183:43–50
- Hochella MF Jr, Brown GE Jr, Ross FK, Gibbs GV (1979) High-temperature crystal chemistry of hydrous Mg- and Fe-cordierite. *Min Mag* 64:337–351
- Ildefonse P, Calas G, Flank A-M, Lagarde P (1995) Low Z elements (Mg, Al, and Si) *K*-edge X-ray absorption spectroscopy in minerals and disordered systems. *Nucl Instr Meth B* 97:172–175
- Ildefonse P, Cabaret D, Sainctavit P, Calas G, Flank A-M, Lagarde P (1998) Local aluminium environment in Earth's surface minerals. *Phys Chem Miner* 25:112–121
- Jackson WE, Farges F, Yeager M, Mabrouk PA, Rossano S, Waychunas GA, Solomon EI, Brown GE Jr (2005) Multi-spectroscopic study of Fe(II) in silicate glasses: implications for the coordination environment of Fe(II) in silicate melts. *Geochimica and Cosmochimica Acta* 69:4315–4332
- Jallot E (2003) Role of magnesium during spontaneous formation of a calcium phosphate layer at the periphery of a bioactive glass coating doped with MgO. *Appl Surf Sci* 211:89–95
- Kas JJ, Sorini P, Prange MP, Cambell LW, Soininen JA, Rehr JJ (2007) Many-pole model of inelastic losses in X-ray absorption spectra. *Phys Rev B* 76:195116–195126
- Kleinman L, Bylander DM (1982) Efficacious form for model pseudopotentials. *Phys Rev Lett* 48(20):1425–1428 doi:10.1103/PhysRevLett.48.1425
- Koenderink GH, Brzesowsky RH, Balkenende AR (2000) Effect of the initial stages of the leaching on the surface of the alkaline earth sodium silicate glasses. *J Non-Cryst Solids* 262:80–98
- Kroeker S, Stebbins JF (2000) Magnesium coordination environments in glasses and minerals: new insight from high-field magnesium-25 MAS NMR. *Am Mineral* 85:1459–1464
- Kubicki JD, Lasaga AC (1991) Molecular dynamics simulation of pressure and temperature effects on MgSiO₃ and Mg₂SiO₃ melts and glasses. *Phys Chem Miner* 17:661–673
- Lefrère Y (2002) Propriétés d'absorption optique du Fe²⁺ et du Fe³⁺ dans des verres d'intérêt industriel: mesure, modélisation et implications structurales. PhD thesis, Université Denis Diderot
- Levelut C, Cabaret D, Benoit M, Jund P, Flank A-M (2001) Multiple scattering calculations of the XANES Si *K*-edge in amorphous silica. *J Non-Cryst Solids* 293:295:100–104
- Li D, Bancroft GM, Fleet ME, Feng XH (1995) Silicon *K*-edge XANES spectra of silicate minerals. *Phys Chem Miner* 22:115–122
- Li D, Peng M, Murata T (1999) Coordination and local structure of magnesium in silicate minerals and glasses: Mg *K*-edge XANES study. *Can Mineral* 37:199–206
- Mizoguchia T, Tatsumi K, Tanaka I (2006) Peak assignments of ELNES and XANES using overlap population diagrams. *Ultra-microscopy* 106:1120–1128
- Mo S-D, Ching W-Y (2000) Ab initio calculation of the core-hole effect in the electron energy-loss near-edge structure. *Phys Rev B* 62:7901–7907
- Monkhorst HJ, Pack JD (1976) Special points for Brillouin-zone integrations. *Phys Rev B* 13:5188–5192
- Mysen B, Richet P (2005) Silicate glasses and melts: properties and structure, vol 10, 2 edn. Elsevier
- Natoli CR (1984) Distance dependence of continuum and bound state of excitonic resonances in X-ray absorption near-edge structures (XANES). In: Hodgson KO, Herman B, PennerHahn JE (eds) EXAFS and Near Edge Structure III. Springer Proceedings on Physics, vol 2, pp 38–42
- Neuville DR, Cormier L, Flank A-M, Briois V, Massiot D (2004) Al speciation and Ca environment in calcium aluminosilicate glasses and crystals by Al and Ca *K*-edge X-ray absorption spectroscopy. *Chem Geol* 213:153–163
- Nord AG, Kierkegaard P (1968) The crystal structure of Mg₃(PO₄)₂. *Acta Chem Scand* 22:1466–1474
- O'Neill HS, Eggins SM (2002) The effect of melt composition on trace element partitioning: an experimental investigation of the activity coefficients of FeO, NiO, CoO, MoO₂ and MoO₃ in silicate melts. *Chem Geol* 186:151–181
- Perdikatsis B, Burzlaff H (1981) Strukturverfeinerung am Talk Mg₃[(OH)₂Si₄O₁₀]. *Zeitschrift für Kristallographie* 156: 177–186
- Pouchou J-L, Pichoir F (1984) Extension of quantitative possibilities of microanalysis by a new formulation of matrix effects. *Journal de Physique (Paris), Colloque* 45(2):17–20
- Quartieri S, Boscherini F, Dalconi C, Iezzi G, Meneghini C, Oberti R (2008) Magnesium *K*-edge EXAFS study of bond-length behavior in synthetic pyrope-grossular garnet solid solutions. *Am Mineral* 93:495–498
- Robinson K, Gibbs GV, Ribbe PH (1971) Quadratic elongation: A quantitative measure of distortion in coordination polyhedra. *Science* 172:567–570
- Rossano S, Behrens H, Wilke M (2008) Advanced analyses of ⁵⁷Fe Mössbauer data of aluminosilicate glasses. *Phys Chem Miner* 35:77–93
- Sánchez del Río M, Suárez M, García Romero, Alianelli L, Felici R, Martinetto EP, Dooryhée E, Reyes-Valerio C, Borgatti F, Doyle B, Giglia A, Mahne N, Pedio M, Nannarone S (2005) Mg *K*-edge XANES of sepiolite and palygorskite. *Nucl Instr Meth Phys Res B* 238:55–60
- Sharp T, Wu Z, Seifert F, Poe B, Doerr M, Paris E (1996) Distinction between six- and fourfold coordinated silicon in SiO₂ polymorphs via electron loss near edge structure (ELNES) spectroscopy. *Phys Chem Miner* 23:17–24
- Sharp ZD, Hazen RM, Finger LW (1987) High-pressure crystal chemistry of monticellite, CaMgSiO₄. *Am Mineral* 72:748–755
- Shimoda K, Tobu Y, Hatakeyama M, Nemoto T, Saito K (2007) Structural investigation of Mg local environments in silicate glasses by ultra-high field ²⁵Mg 3QMAS NMR spectroscopy. *Am Mineral* 92:695–698
- Shiono T, Minagi T, Aritani H, Okumura S, Nishida T (2002) Mg *K*-edge XANES study of crystallization of MgAl₂O₄ spinel prepared from a mixture of Al(OH)₃ and Mg(OH)₂ activated mechanically by wet milling. *UVSOR Act Rep* 2001:192–193
- Stephenson DA, Moore PB (1968) The crystal structure of grandierite, (Mg,Fe)Al₃SiO₉. *Acta Cryst B* 24:1518–1522
- Taillefumier M, Cabaret D, Flank A-M, Mauri F (2002) X-ray absorption near-edge structure calculations with the pseudopotentials: application to the *K* edge in diamond and alpha-quartz. *Phys Rev B* 66:195107(1–8)
- Thompson A, Attwood D, Gullikson E, Howells M, Kim K-J, Kirz J, Kortright J, Lindau I, Pianetta P, Robinson A, Scofield J, Underwood J, Vaughan D, Williams G, Winick H (2001) X-ray

- data booklet. LNBL, Berkeley, USA, 2001. Center for X-ray Optics and Advanced Light Source
- Toplis MJ (2005) The thermodynamics of iron and magnesium partitioning between olivine and liquid: criteria for assessing and predicting equilibrium in natural and experimental systems. *Contrib Mineral Petrol* 149:22–39
- Trcera N, Cabaret D, Farges F, Flank A-M, Lagarde P, Rossano S (2007) Mg *K*-edge XANES spectra in crystals and oxide glasses: experimental vs. theoretical approaches. In: Hedman B, Pianetta P (eds) X-ray absorption fine structure—XAFS13, AIP Conference Proceedings, vol 882, pp 226–228
- Troullier N, Martins JL (1991) Efficient pseudopotentials for plane-wave calculations. II. Operators for fast iterative diagonalization. *Phys Rev B* 43(11):8861–8869
- Wilding MC, Benmore CJ, Tangeman JA, Sampath S (2004) Coordination changes in magnesium silicate glasses. *Europhys Lett* 67(2):212–218
- Winterer M (1997) XAFS—a data analysis program for materials science. *J Phys IV* 7 C2:243–244
- Wu ZY, Mottana A, Paris E, Giuli G, Cibin G (2004) X-ray absorption near-edge structure at the Mg *K*-edge in olivine minerals. *Phys Rev B* 69:104106
- Yamanaka T, Takeuchi Y (1983) Order-disorder transition in MgAl₂O₃ spinel at high temperatures up to 1700°C. *Zeitschrift für Kristallographie* 165:65–78